Supporting Information

Carbon-Modulated Reduction Synthesis of Dual-Valent Eu-Doped $La_3Si_2O_8Cl$ Phosphors: Single-Matrix White LEDs and High-Resolution Solar-Blind UV Detection

Xinhan Chen,[a] *Gaofan Chen,*[a] *Ya-Nan Feng,*[a] *Lizhen Zhang,*[b,*] *Yan Yu* [a] *and Lingyun Li* [a,*]

[a] Key Laboratory of Advanced Materials Technologies, International (HongKong Macao and Taiwan) Joint Laboratory on Advanced Materials Technologies, College of Materials Science and Engineering, Fuzhou University, No.2 Wu Long Jiang North Avenue, Fuzhou, Fujian, 350108, China. E-mail: lilingyun@fzu.edu.cn

[b] Key Laboratory of Optoelectronic Materials Chemistry and Physics, Fujian Institute of Research on the Structure of Matter, Chinese Academy of Sciences, Fuzhou, Fujian, Fuzhou 350002, China. E-mail: lzzhang@fjirsm.ac.cn

Table of Content

Table S1. The second-order exponential fitting results of LSOCl:7%Eu (Eu:C = 1:0 to 1:2.4) monitored at 505 nm.

sample	A_1	τ_1	A_2	τ_2	τ_{av}(μs)	R^2
Eu:C = 1:0	705	0.259	1045	1.11	0.99	0.998
Eu:C = 1:1.4	870	0.2	1083	0.981	0.87	0.999
Eu:C = 1:1.7	1111	0.26	836	1	0.81	0.999
Eu:C = 1:1.9	627	0.345	1029	1.025	0.91	0.999
Eu:C = 1:2.4	945	0.24	958	1.004	0.86	0.999

Table S2. The first-order exponential fitting results of LSOCl:7%Eu (Eu:C = 1:0 to 1:2.4) monitored at 613 nm.

sample	τ1(ms)	R^2
Eu:C = 1:0	1.49	0.99661
Eu:C = 1:1.4	1.47	0.99622
Eu:C = 1:1.7	1.47	0.99576
Eu:C = 1:1.9	1.44	0.99516
Eu:C = 1:2.4	1.46	0.99658

Table S3. The formation energy of Eu occupying different lattice sites in LSOCl

Dopants	La1 site	La2 site
Eu^{3+}	5.23 eV	5.20 eV
Eu^{2+}	1.31 eV	1.31 eV

NOTE：

We performed first-principles simulations to investigate Eu^{2+}/Eu^{3+} occupancy preferences using density functional theory (DFT) implemented in the Vienna Ab initio Simulation Package (VASP)[**R1**]. The exchange-correlation functional was treated with the Perdew-Burke-Ernzerhof (PBE)[**R3**] generalized gradient approximation (GGA)[**R2**], employing a 700 eV plane-wave cutoff energy. A 3×5×7 Monkhorst-Pack k-mesh sampled the Brillouin zone, with structural relaxations converging to atomic forces $<10^{-2}$ eV/Å and energy differences $<10^{-6}$ eV. The formation energy is calculated according to the following formula:

$$E_f = E_{doped} - E_{pure} + E_{site} - E_{atom}$$

where E_{doped} is the energy of the doped cell, E_{pure} is the energy of the initial cell, E_{site} is the energy of the replaced element, and E_{atom} is the energy of the doped element. As summarized in **Table S3**, Eu^{2+} incorporation shows equivalent formation energies (1.31 eV) at both La sites, predicting statistical distribution between La1 and La2 positions.

References

[R1] G. Kresse,J. Furthmüller. Efficient iterative schemes for ab initio total-energy calculations using a plane-wave basis set[J]. Phys. Rev. B, 1996, 54(16): 11169-11186.

[R2] G. Kresse,D. Joubert. From ultrasoft pseudopotentials to the projector augmented-wave method[J]. Phys. Rev. B, 1999, 59(3): 1758-1775.

[R3] P. E. Blöchl. Projector augmented-wave method[J]. Phys. Rev. B, 1994, 50(24): 17953-17979.

Table S4. CIE coordinates and offset rates of LSOCl:7%Eu Eu:C = 1:1.4

Excitation wavelength/nm	**（*x*，*y*）**	***x* offset rate**	***y* offset rate**	**Total offset rate**
250	(0.61,0.35)	0.00%	0.00%	0.00%
254	(0.61,0.35)	0.00%	0.00%	0.00%
260	(0.62,0.35)	1.64%	0.00%	1.64%
270	(0.61,0.35)	0.00%	0.00%	0.00%
280	(0.58,0.35)	4.92%	0.00%	4.92%
290	(0.54,0.35)	11.48%	0.00%	11.48%
300	(0.49,0.34)	19.67%	2.86%	22.53%
302	(0.47,0.34)	22.95%	2.86%	25.81%
310	(0.41,0.33)	32.79%	5.71%	38.50%
320	(0.35,0.33)	42.62%	5.71%	48.34%
330	(0.29,0.32)	52.46%	8.57%	61.03%
340	(0.27,0.33)	55.74%	5.71%	61.45%
350	(0.26,0.33)	57.38%	5.71%	63.09%
360	(0.39,0.34)	36.07%	2.86%	38.92%
365	(0.30,0.34)	50.82%	2.86%	53.68%

Table S5. CIE coordinates and offset rates under different excitation wavelengths of LSOCl:7%Eu Eu:C = 1:1.4

Excitation wavelength/nm	**（*x*，*y*）**	***x* offset rate**	***y* offset rate**	**Total offset rate**
254	(0.63,0.35)	0.00%	0.00%	0.00%
254,302	(0.57,0.35)	9.52%	0.00%	9.52%
254,365	(0.55,0.34)	12.70%	2.86%	15.56%
254,302,365	(0.52,0.34)	17.46%	2.86%	20.32%

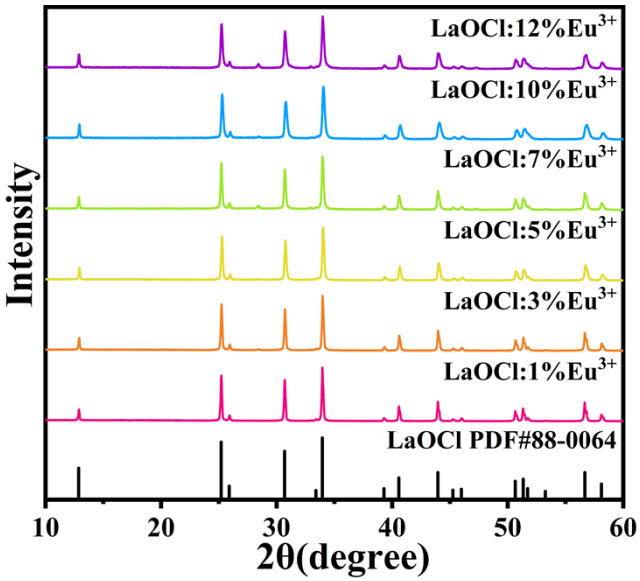

Figure S1. PXRD patterns of LaOCl:x%Eu^{3+} (x = 1 to 12), and standard patterns of PDF card No. 88-0064 for LaOCl as the reference.

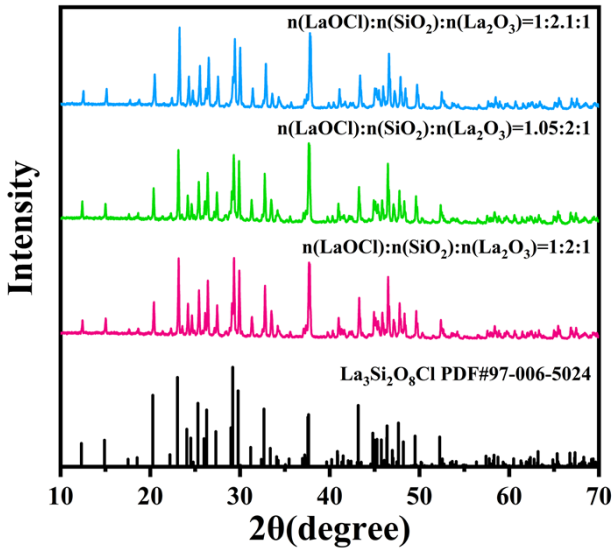

Figure S2. XRD patterns of LSOCl synthesized at different stoichiometric ratios, and standard patterns of PDF card No. 97-006-5024 for LSOCl as the reference.

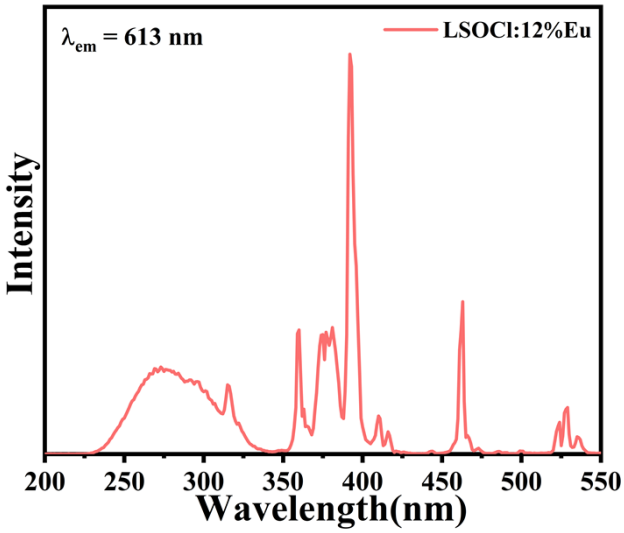

Figure S3. Excitation spectra of LSOCl:12%Eu (monitored at 613 nm).

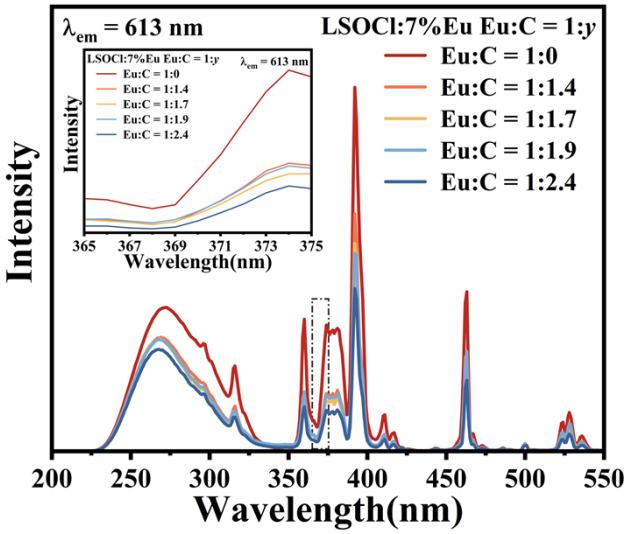

Figure S4. Excitation spectra of LSOCl:7%Eu (Eu:C = 1:0 to 1:2.4). The inset is an enlarged image of 365-375 nm.

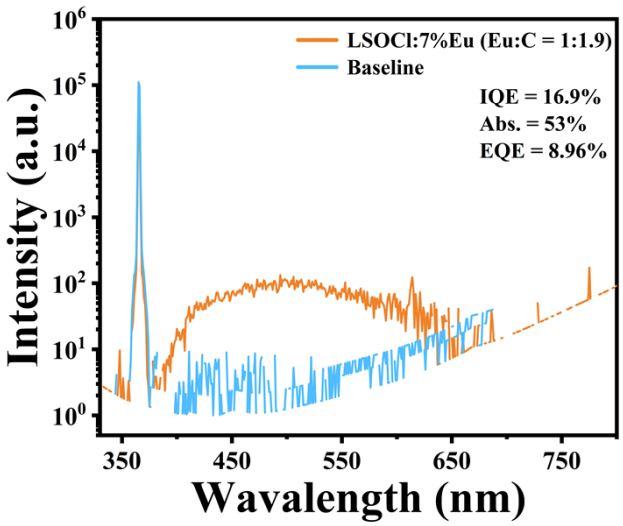

Figure S5. Measurement and spectral analysis of the internal quantum efficiency of LSOCl:7%Eu (Eu:C = 1:1.9)

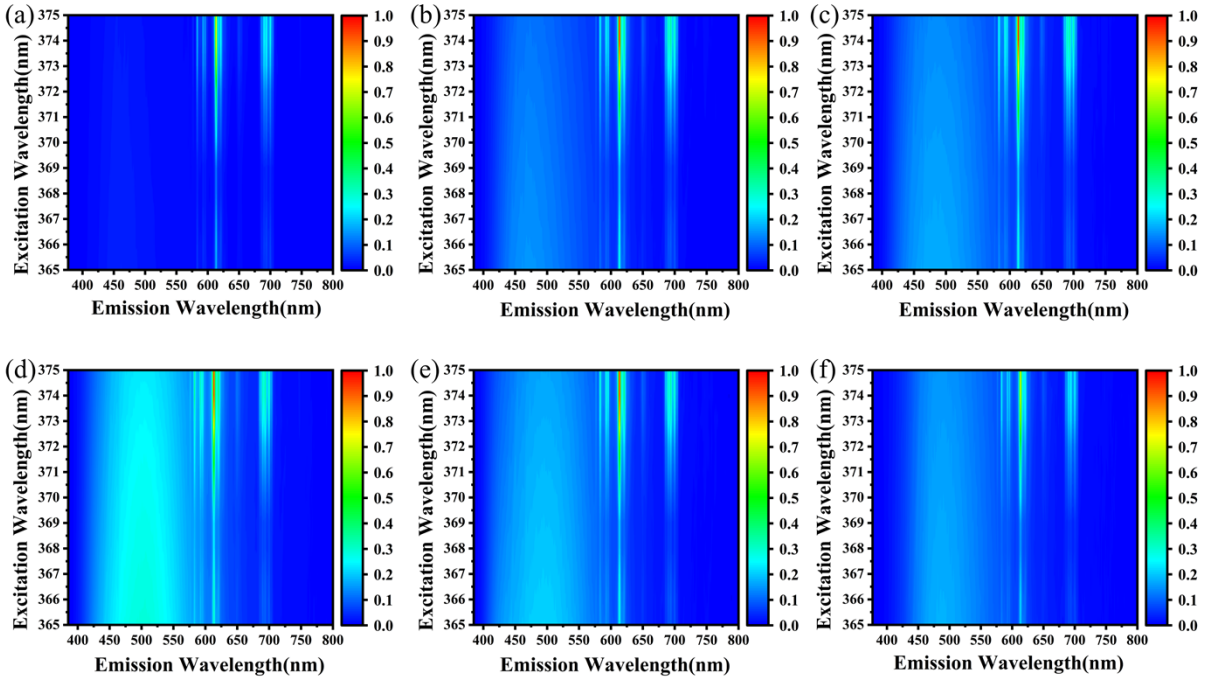

Figure S6. Excitation-dependent emission spectra of LSOCl:7%Eu Eu:C = 1:0 (a). Eu:C = 1:1.2 (b). Eu:C = 1:1.4 (c). Eu:C = 1:1.7 (d). Eu:C = 1:2.1 (e). Eu:C = 1:2.4 (f).

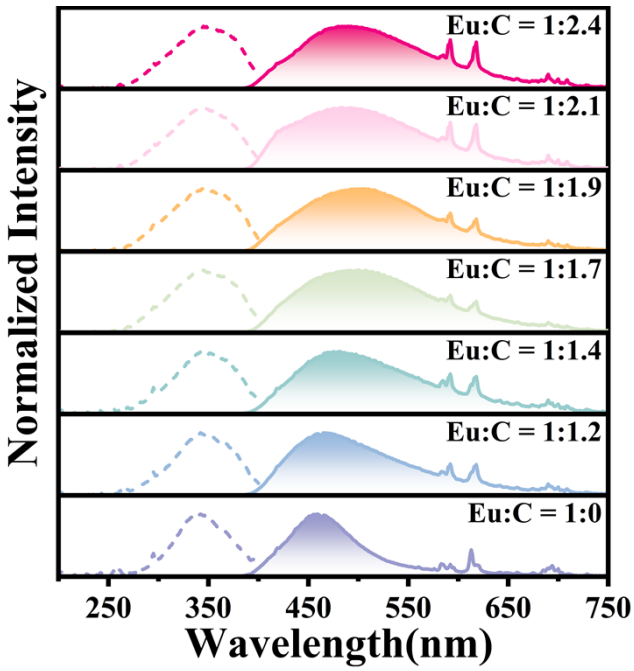

Figure S7. Excitation and emission spectra of LSOCl:7%Eu (Eu:C = 1:0 to 1:2.4) (λ_{ex} = 345 nm, λ_{em}= 500 nm).

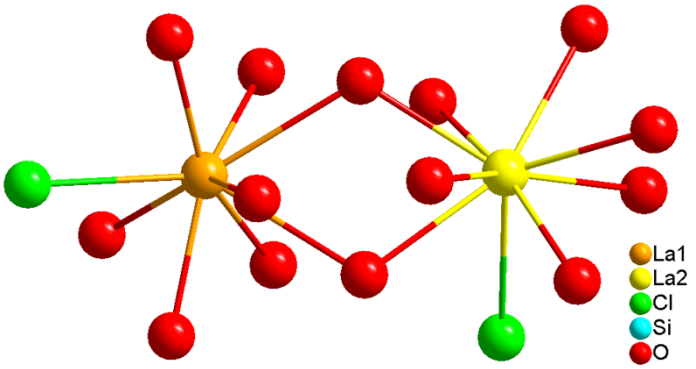

Figure S8. Coordination of La1 and La2 atoms in $La_3Si_2O_8Cl$.

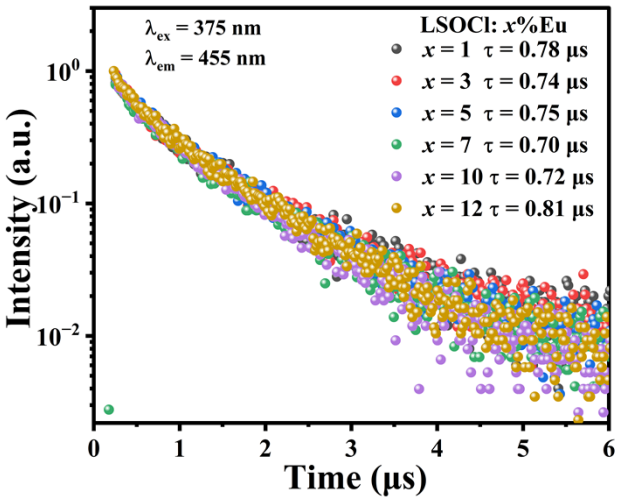

Figure S9. Luminescence decay curves of LSOCl:*x*%Eu (*x* = 1, 3, 5, 7, 10, 12) monitored at 455 nm.

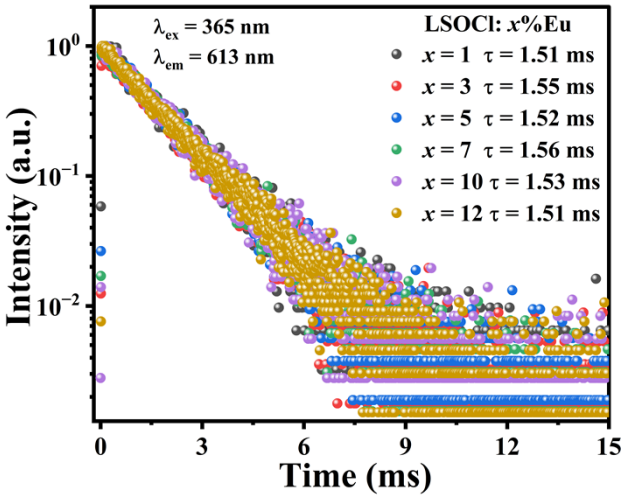

Figure S10. Luminescence decay curves of LSOCl:*x*%Eu (*x* = 1, 3, 5, 7, 10, 12) monitored at 613 nm.

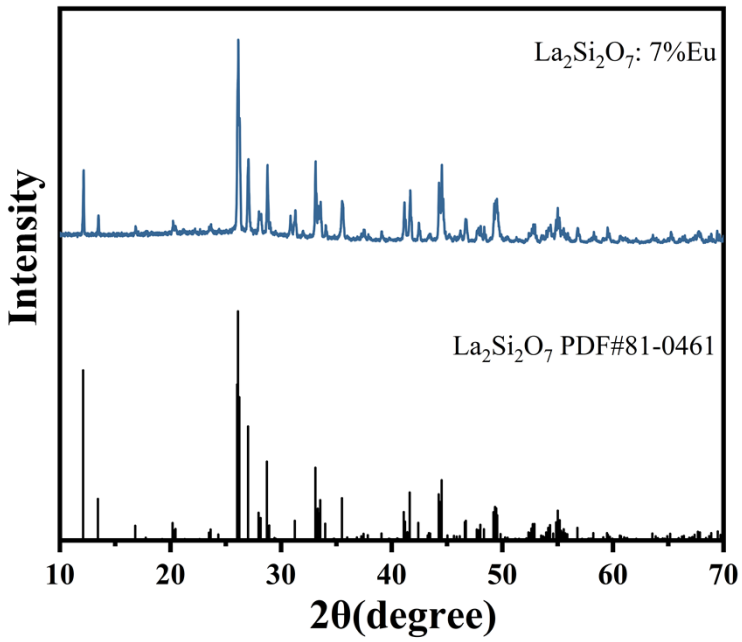

Figure S11. PXRD patterns of $La_2Si_2O_7$:7%Eu phosphor, and standard patterns of PDF card No. 81-0461 for $La_2Si_2O_7$ as the reference.

(**Note** : The raw materials used include La_2O_3, SiO_2 and Eu_2O_3. The samples were prepared by two rounds of sintering. The first round of sintering was carried out in an air atmosphere. The raw materials were placed in a muffle furnace, heated to 1350 °C for 1300 min, and held for 360 min to obtain $La_2Si_2O_7$:7%Eu^{3+} sample. The second round of sintering was carried out in a reducing atmosphere created by carbon powder. Similarly, in a muffle furnace, after 400 min heating up to 1350 °C and holding for 360 min, the $La_2Si_2O_7$:7%Eu samples were finally obtained.)

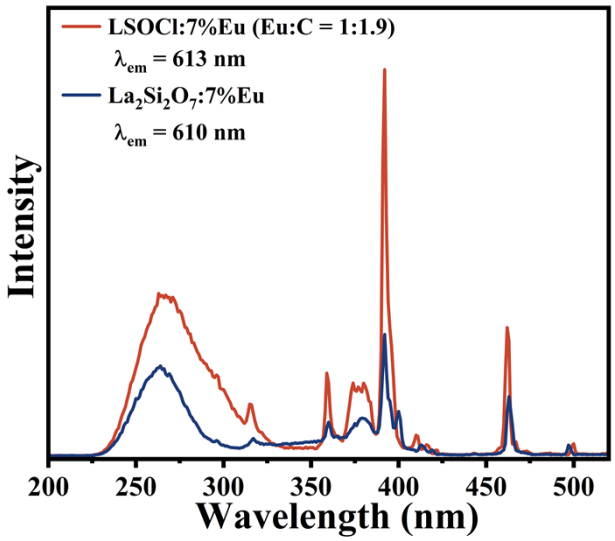

Figure S12. Excitaton spectra of $La_2Si_2O_7$:7%Eu and $La_3Si_2O_8Cl$:7%Eu (Eu:C=1:9).

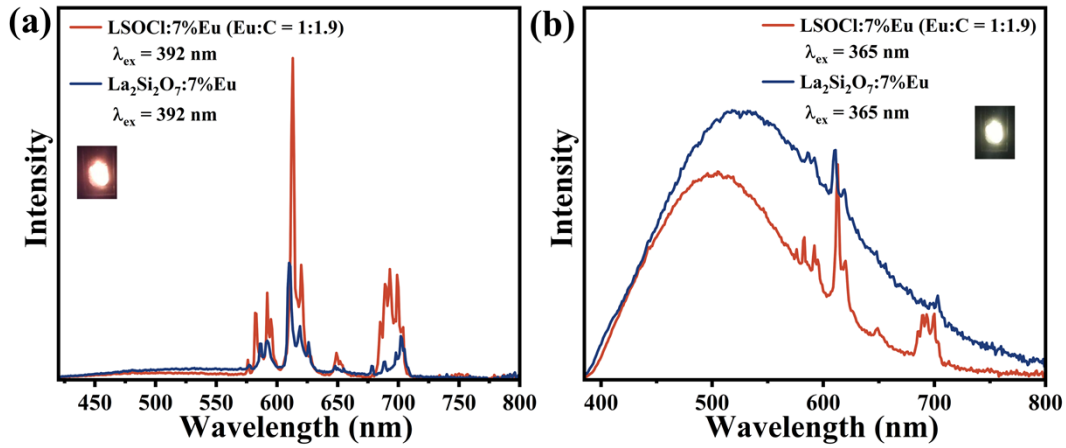

Figure S13. Photo luminescence spectra of $La_2Si_2O_7$:7%Eu and $La_3Si_2O_8Cl$:7%Eu (Eu:C=1:9) excited at 392 nm (a) and 365 nm (b).

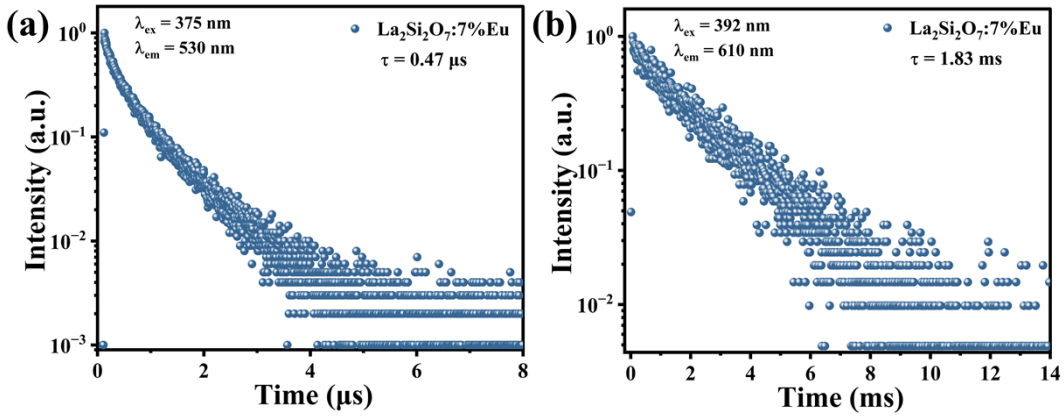

Figure S14. Photo luminescence spectra of $La_2Si_2O_7$:7%Eu and $La_3Si_2O_8Cl$:7%Eu (Eu:C=1:9) excited at 392 nm (a) and 365 nm (b).

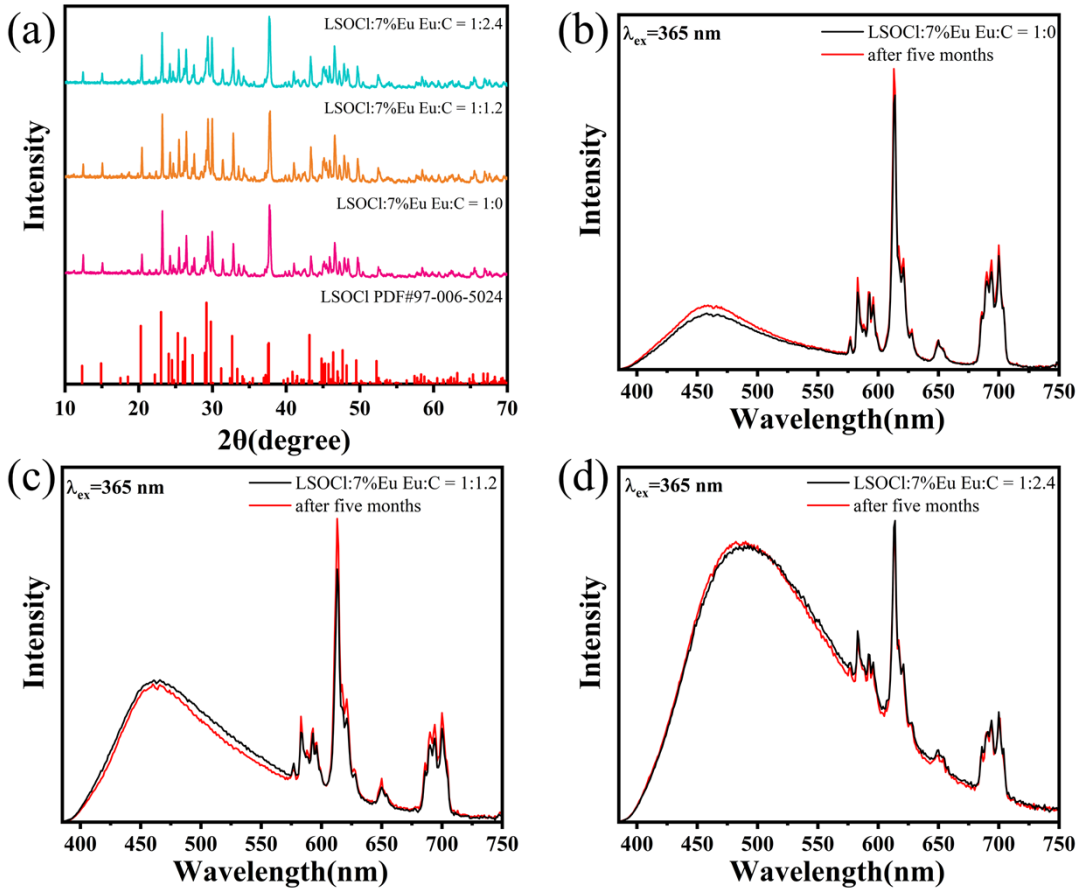

Figure S15. PXRD patterns of LSOCl:7%Eu (Eu:C = 1:0, 1:1.2, and 1:2.4) (a) emission spectra (b-d) after being exposed in ambient air for five months.

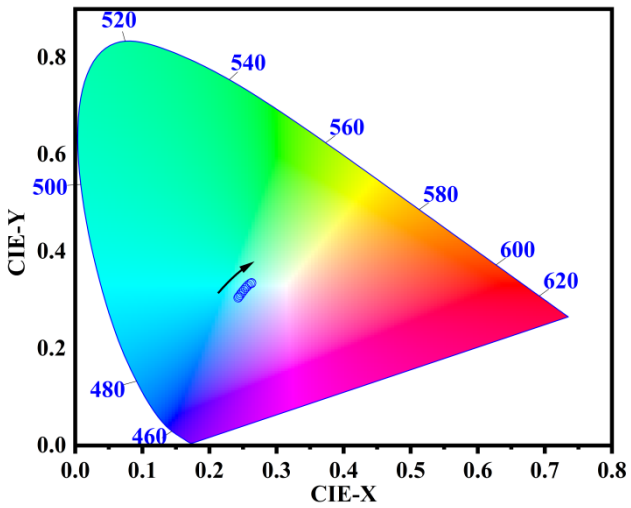

Figure S16. Temperature-dependent CIE color coordinates of LSOCl:7%Eu (Eu:C = 1:1.9) at temperature ranges of 80-300 K.

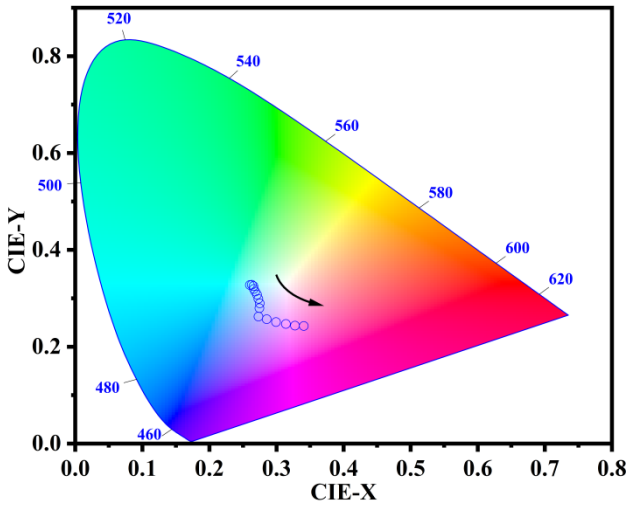

Figure S17. Temperature-dependent CIE color coordinates of LSOCl:7%Eu (Eu:C = 1:1.9) at temperature ranges of 300-578 K.

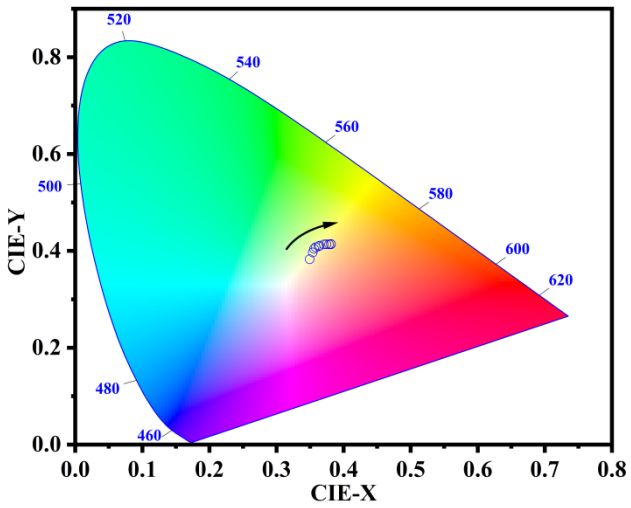

Figure S18. Current-dependent CIE color coordinates of the WLED based on LSOCl:7%Eu (Eu:C = 1:1.9)

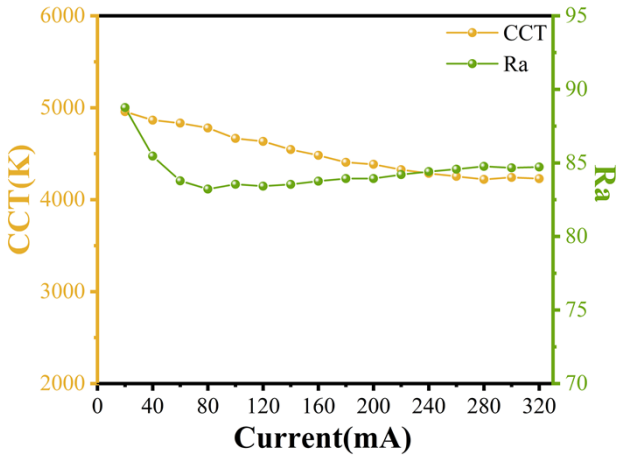

Figure S19. CCT and Ra of the WLED based on LSOCl:7%Eu (Eu:C = 1:1.9) under different applied current.

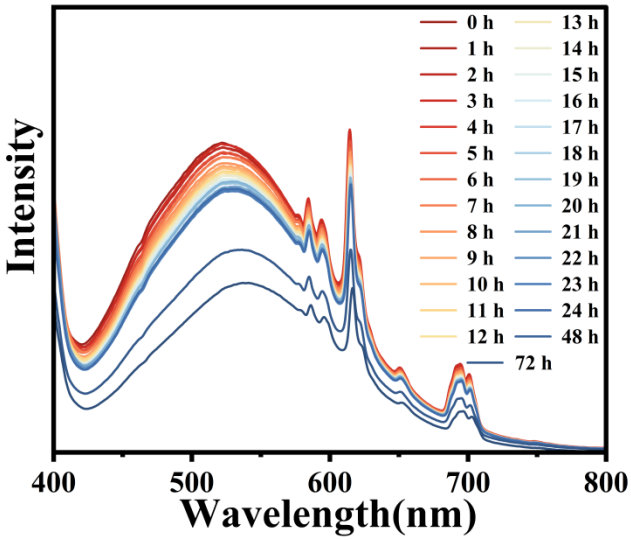

Figure S20. The emission spectra of the WLED based on LSOCl:7%Eu (Eu:C = 1:1.9) under seventy-two hours of continuous operation.

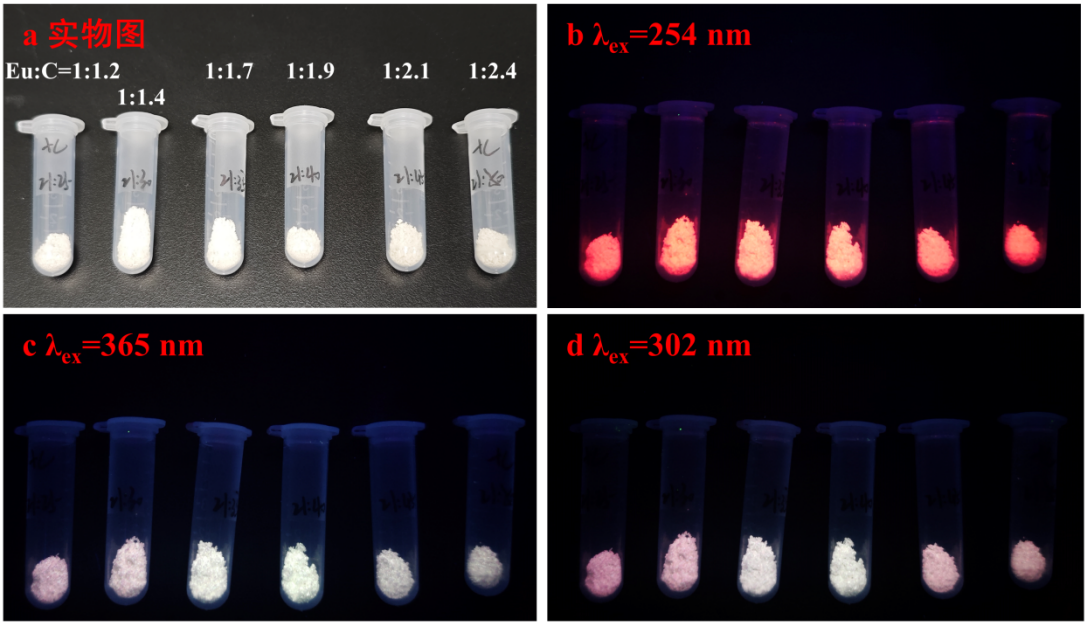

Figure S21. Photograph of LSOCl:7%Eu (Eu:C = 1:0 to 1:2.4)

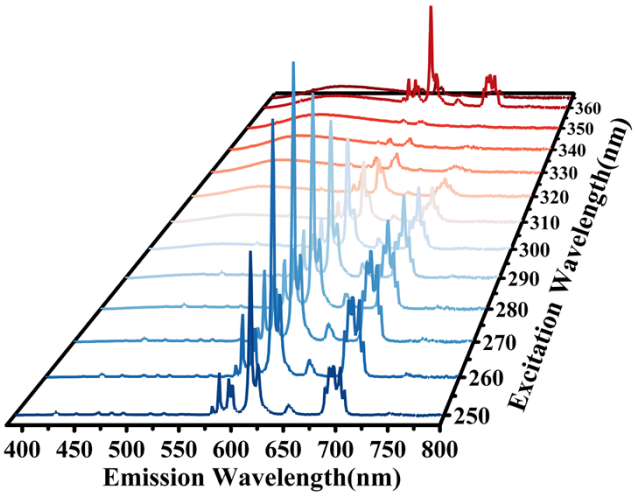

Figure S22. Excitation-dependent emission spectra of LSOCl:7%Eu Eu:C = 1:1.4 (λ_{ex} = 250-365 nm).